

Magnetic states of Ni-Mn-Sn based shape memory alloy: a combined muon spin relaxation and neutron diffraction study

J. Sannigrahi¹, S. Pramanick², S. Chatterjee³, J. S. Lord¹, D.

Khalyavin¹, A.D. Hillier¹, D. T. Adroja^{1,4}, S. Majumdar^{3*}

¹ISIS Neutron and Muon Source, Science and Technology Facilities Council,
Rutherford Appleton Laboratory, Didcot OX11 0QX, United Kingdom

²UGC-DAE Consortium for Scientific Research, Kolkata Centre,
Sector III, LB-8, Salt Lake, Kolkata 700 098, India

³School of Physical Sciences, Indian Association for the Cultivation of Science,
2A & B Raja S. C. Mullick Road, Jadavpur, Kolkata 700 032, India and

⁴Highly Correlated Matter Research Group, Physics Department,
University of Johannesburg, Auckland Park 2006, South Africa

The fascinating multiple magnetic states observed in the Ni-Mn-Sn based metamagnetic shape memory alloy are addressed through a combined muon spin relaxation (μ SR) and neutron powder diffraction studies. The material used in the present investigation is an off-stoichiometric alloy of nominal composition, $\text{Ni}_{2.04}\text{Mn}_{1.4}\text{Sn}_{0.56}$. This prototypical alloy, similar to other members in the Ni-Mn-Sn series, orders ferromagnetically below T_{CA} ($= 320$ K), and undergoes martensitic type structural transition at T_{MS} ($= 290$ K), which is associated with the sudden loss of magnetization. The sample regains its magnetization below another magnetic transition at $T_{CM} = 260$ K. Eventually, the composition shows a step-like anomaly at $T_B = 120$ K, which is found to coincide with the blocking temperature of exchange bias effect observed in the alloy. In our study, the initial asymmetry (A_{10}) of the μ SR data falls rapidly below T_{CA} , indicating the onset of bulk magnetic order. A_{10} regains its full asymmetry value below T_{MS} suggesting the collapse of the ferromagnetic order into a fully disordered paramagnetic state. Below the second magnetic transition at T_{CM} , asymmetry drops again, confirming the re-entrance of a long range ordered state. Interestingly, A_{10} increases sluggishly below T_B , indicating that the system attains a disordered/glassy magnetic phase below T_B , which is responsible for the exchange bias and frequency dispersion in the ac susceptibility data as previously reported. The neutron powder diffraction data do not show any magnetic superlattice reflections, ruling out the possibility of a long range antiferromagnetic state at low temperatures. The ground state is likely to be comprised of a concentrated metallic spin-glass in the backdrop of an ordered ferromagnetic state.

I. INTRODUCTION

Advanced functional materials play an ever increasing role in the modern technological developments, which encompass areas such as energy harvesting, computation, communication as well as to combat environmental pollution. Broadly, they can be classified into five groups depending upon their functionality; Adaptive, Magnetic, Electric, Optical, and Energy and Environmental materials. It is needless to mention that a proper investigation of their physical properties is important in understanding the essential physics associated with their functionality. For example, the study of CuO-based high T_C superconductors has enriched our understanding of electronic properties of correlated metal oxides. It is to be noted that many of these functional materials are actually multifunctional, *i.e.*, they show two or more functional properties. $\text{Ni}_{2.04}\text{Mn}_{1.4}\text{Sn}_{0.56}$, the title composition of this work, is one such material having functionality as adaptive, magnetic, electric as well as energy and environmental material.

$\text{Ni}_{2.04}\text{Mn}_{1.4}\text{Sn}_{0.56}$ belongs to a class of materials known as metamagnetic shape memory alloys (MSMAs). They show large magnetic field induced strain, magneto-resistance, magneto-caloric, baro-caloric, and exchange

bias effects.^{1–6} The general compositions of these alloys can be expressed as $\text{Ni}_2\text{Mn}_{1+p}\text{Z}_{1-p}$ ($\text{Z} = \text{In, Sn, Sb}$ and $p < 1$), and the observed functionality arises from their bi-ferroic nature with the simultaneous presence (as well as their mutual interplay) of ferromagnetism and ferroelasticity. The alloys are characterized by first-order martensitic type structural phase transition occurring at a temperature T_{MS} and a second order paramagnetic (PM) to ferromagnetic (FM) transition at the Curie point (T_C). For the practical realization of magnetic shape memory and other magneto-functional properties, one should have $T_C > T_{MS}$, *i.e.*, the sample should be in a magnetically ordered state when martensitic phase transition (MPT) takes place.

The presence of two critical temperatures (namely T_C and T_{MS}) makes the system to have a rather exotic phase diagram. There are few important aspects associated with these alloys, which remain elusive till date. Firstly, what happens to the FM state of the alloy (we are considering $T_C > T_{MS}$) right below the MPT? The high temperature structural phase is called austenite with cubic lattice symmetry, while the low temperature phase (below T_{MS}) is called martensite with a tetragonal/orthorhombic/modulated structure. It is found that magnetization drops sharply below T_{MS} , indicating the loss of ordered FM moment. Some diffuse peaks were ob-

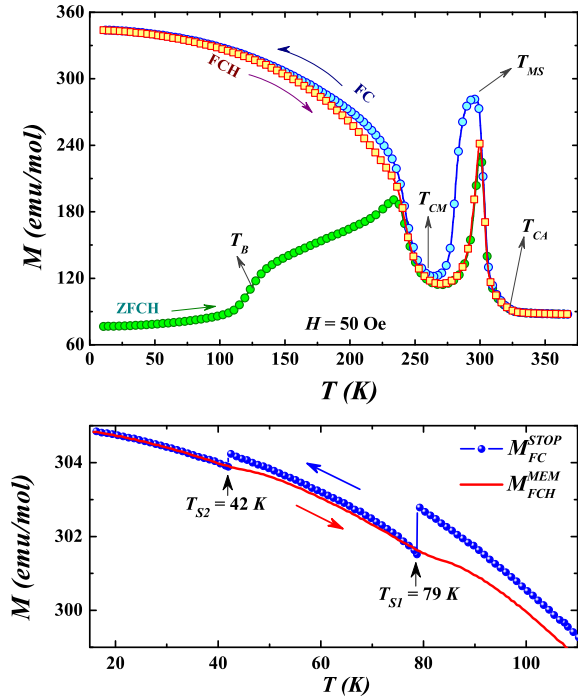


FIG. 1. In the upper panel, magnetization is plotted as a function of temperature in zero-field-cooled heating (ZFCH), field cooling (FC) and field-cooled heating (FCH) conditions in presence of 50 Oe of external magnetic field. The martensitic transformation (T_{MS}) is clearly visible around 300 K, where large thermal hysteresis is present. T_{CA} , T_{CM} and T_B indicate austenite Curie point, martensite Curie point and exchange bias blocking temperature respectively. The lower panel shows the field-cooled-field-stop memory data indicating the presence of glassy magnetic phase below 120 K. Here M_{FC}^{STOP} denotes the magnetization data recorded during cooling along with 1 h stops at 80 K and 40 K. Magnetic field was turned off during the stops. M_{FCH}^{MEM} denotes the subsequent heating run, and clear anomalies (in the form of shallow dips) were observed at the stopping points signifying the presence of memory.

served in the Neutron Powder Diffraction (NPD) data of Ni-Mn-Sn alloys, which were assigned to the existence of incipient antiferromagnetic (AFM) coupling⁷. As evident from the chemical compositions, a fraction of Z atoms is replaced by Mn (we call it Mn'), and theoretical calculations indicate the existence of AFM correlation between regular Mn and Mn' atoms.^{8–14} On the other hand, ⁵⁷Co-Rh Mössbauer spectroscopy on a Ni-Mn-Sn alloy (with small amount of enriched ⁵⁷Fe doped at the Mn site) indicated a PM state below T_{MS} of the sample.¹⁵ NPD studies, performed on various Ni-Mn-Z alloys, fail to identify well defined magnetic Bragg peaks associated with an ordered AFM state.^{7,16} Neutron polarization study indicates the existence of FM correlations, which vanishes below T_{MS} with the concomitant occurrence of Mn-Mn' AFM correlations.¹⁷ Therefore, the nature of the magnetic state just below T_{MS} remains uncertain; it may be

incipient AFM in the backdrop of a PM/FM phase, a long range ordered AFM state with weak moment or an FM state with reduced Mn moment.

The second unresolved point is associated with the magnetic ground state of these alloys. The off-stoichiometric Ni-Mn-Z alloys show a step-like feature well below T_{MS} in the zero-field-cooled magnetization data and exchange bias (EB) effect was observed below T_B . Our group previously reported that field-cooling from just above T_B is sufficient to observe EB, and T_B actually signifies a spin freezing temperature.¹⁸ Subsequently, there have been numerous reports on the glassy magnetic state of the Ni-Mn-Z alloys.^{19–22} Nevertheless, ambiguities remain on the nature of the glassy state, and the ground state has been described as re-entrant spin glass, cluster glass or super spin glass by various authors (cited in the previous line). EB generally requires two different magnetic phases (say, FM + AFM or spin-glass + FM) to be present. Presence of AFM clusters below T_{MS} is highly possible, since there is a strong evidence for incipient antiferromagnetism. It remains unclear whether the ground state is characterized by a (i) mixture of AFM and FM phase fractions along with interfacial glassiness, (ii) coexisting spin-glass (SG) and FM phases, or (iii) stand alone SG phase.

In the present work, we have addressed these aspects using muon spin resonance/rotation (μ SR) as well as NPD techniques on an MSMA of nominal composition, $\text{Ni}_{2.04}\text{Mn}_{1.4}\text{Sn}_{0.56}$. One can notice that a small amount of excess Ni is doped at the expense of Sn, which is required to elevate T_{MS} . While ferromagnetic Curie point of the high temperature austenite is around $T_{CA} = 320$ K, the structural transition takes place around $T_{MS} = 290$ K. The reason for choosing this composition lies with the fact that T_{MS} is very close to T_{CA} , and the FM state becomes unstable below the MPT (see fig. 1). The sample regains its magnetization below a second transition at $T_{CM} = 260$ K in the martensitic phase. The step like anomaly is seen below $T_B = 120$ K, and considerable EB is observed at low temperature.²³ The sample shows the signature of field-cooled-field-stop memory (FCFS)²⁴ as shown in the lower panel of fig. 1. The observed FCFS in this bulk sample indicates the presence of glassy magnetic ground state.

II. EXPERIMENTAL DETAILS

The polycrystalline sample of $\text{Ni}_{2.04}\text{Mn}_{1.4}\text{Sn}_{0.56}$ for the present study was prepared by argon arc melting the constituent elements.²³ The temperature (T) dependent dc magnetization (M) measurements were performed using a commercial Quantum Design SQUID magnetometer (MPMS 3). The μ SR measurements were performed at ISIS facility, Rutherford Appleton Laboratory, UK using EMU (for zero magnetic field) and HIFI (for longitudinal magnetic field) spectrometers. The sample was mounted on a silver sample holder to minimize the back-

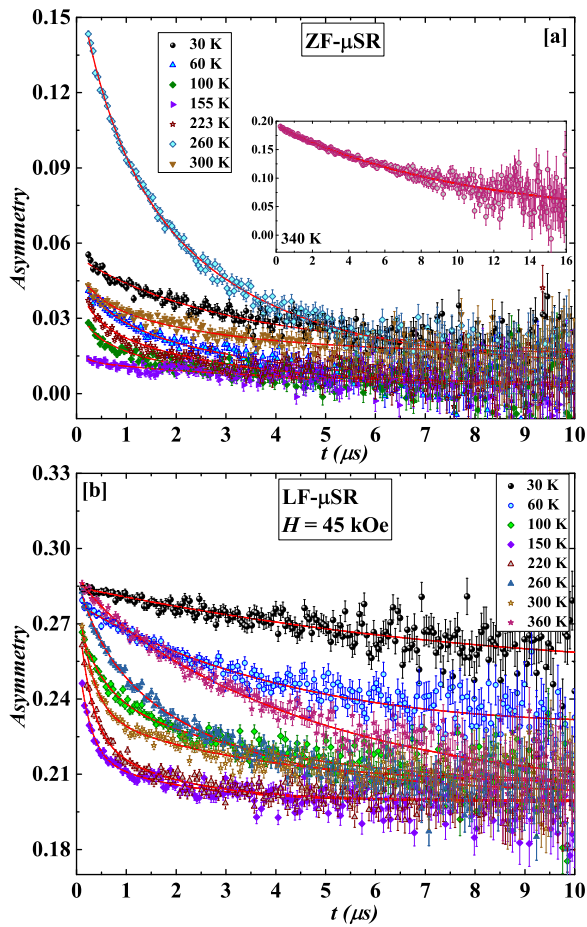


FIG. 2. (a) shows the muon spin relaxation data measured in zero magnetic field at different constant temperatures. The inset shows the same recorded at 340 K, where the sample is in the paramagnetic austenitic phase. (b) depicts the similar data recorded in presence of 45 kOe of applied magnetic field.

ground and measurements were performed at different temperatures. The neutron powder diffraction was carried out at the WISH time of flight diffractometer at the ISIS facility between 8 and 363 K. The powdered sample was inserted in a cylindrical vanadium container of 6 mm diameter. A standard Helium closed cycle refrigerator was used to cool the sample down to 8 K. Nuclear and magnetic structure refinements were performed by the Rietveld method using the FULLPROF program.²⁵ The diffraction peaks were described by a pseudo-Voigt profile function.

III. RESULTS

III.1. Muon Spin Relaxation

μ SR is an accomplished local probe technique to study the magnetism of a material.²⁶ Spin polarized positive muons (μ^+) are implanted into the sample. The implanted muons decay into positrons, which are emitted preferentially in the direction of the muon spin. The spin of the implanted μ^+ precesses around the effective magnetic field vector at the site of implantation. Random and fluctuating fields within the sample can depolarize the muons. In the actual zero field (ZF) or longitudinal field (LF) experiment, the emitted positrons are counted parallel and anti-parallel to the initial muon spin direction. The difference between the number of positrons in the forward and backward directions is generally measured as a function of time (t), and it is called the asymmetry function, $G_z(t)$. Since, $G_z(t)$ is a measure of muon depolarization, one can get significant information on the magnetic state of the material out of it.^{27,28}

For a typical magnetic material, the relaxing part of the asymmetry often obeys an exponential law, $G_z = A_0 \exp(-\lambda t)$, where A_0 is the initial asymmetry, and λ is the (spin-lattice) relaxation rate. For the present Ni-Mn-Sn alloy, the simple exponential law is found to be inadequate to describe the data at all temperatures. The simplest approach is to have a bimodal distribution with two relaxation rates, λ_1 and λ_2 , which results,²⁹

$$G_z(t) = A_{10} \exp(-\lambda_1 t) + A_{20} \exp(-\lambda_2 t) + b_g \quad (1)$$

Here b_g denotes the time independent background of asymmetry. Similar two exponent model has been used for diverse magnetic systems successfully, which include perovskite manganites,^{29–31} cobaltates,³² as well as Heschel based intermetallic alloys.³³ Muons, whose nearest atom on the Z sublattice is either Mn' or Sn, are subject to different internal fields. The regression converges better over full T range, if we put the constrain $A_{20} = 0.4A_{10}$, and the fittings presented in the subsequent parts have been performed considering the above constrain. The value of b_g for a particular fixed magnetic field was estimated from $T = 30$ K data and it is kept constant at all T for a particular value of H . For the ZF case, the value of b_g was kept constant at 0.0094(4), while for the LF data it is fixed at the value 0.1973(4).

Considering glassy ground state in the studied alloy, we have additionally used a stretched exponential function to fit the data below 150 K.^{27,34–37}

$$G_z(t) = A_{10} \exp [(-\lambda t)^\beta] + b_g \quad (2)$$

Here β is called the shape parameter and b_g is the background. Similar to the double exponential fitting, we have kept b_g fixed for all T values for a particular H .

Fig. 2 (a) shows the time domain μ SR data recorded at different temperatures in ZF condition while cooling.

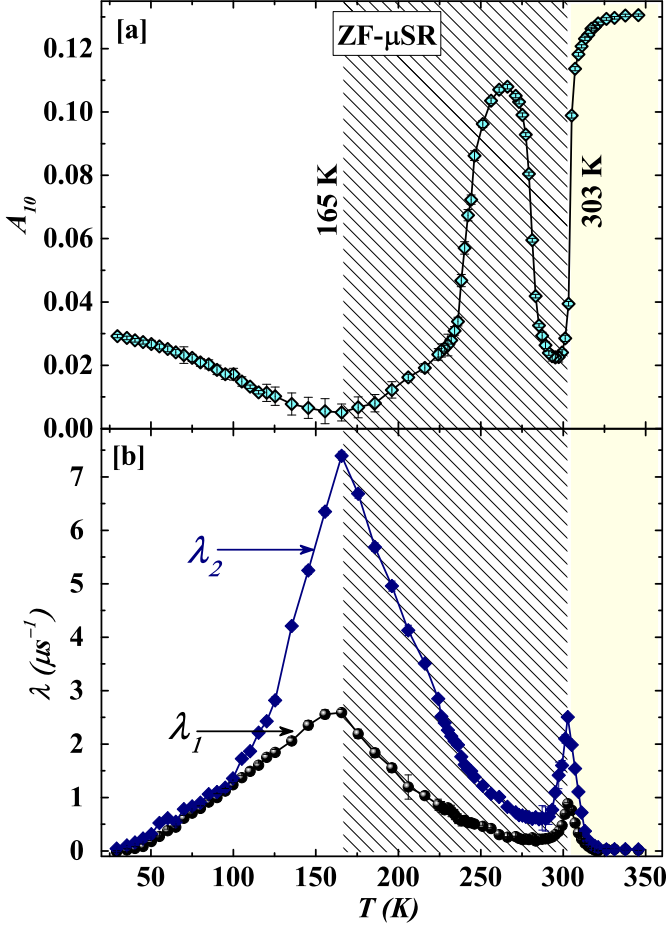


FIG. 3. (a) shows the muon asymmetry, A_{10} as a function of temperature measured in zero magnetic field while cooling. (b) shows the thermal variation of muon depolarization rate, λ_1 and λ_2 at $H = 0$.

At $T = 340$ K, the asymmetry shows an exponential like decay, which is expected for a PM state. On lowering the temperature below the FM Curie point ($T_{CA} = 320$ K), $G_z(t)$ shows a fast relaxation component, which coexists with the slow relaxing part. This is clearly due to the onset of FM transition in the system. On further lowering T below T_{MS} ($= 290$ K), the fast relaxation component appears to get diminished. This corresponds to the rapid fall of M below T_{MS} in the magnetization data [see fig. 1 (a)]. The fast relaxation reappears when the sample is cooled below the second magnetic ordering point T_{CM} . Most interestingly, the damping gradually gets reduced, when the sample is cooled below the blocking temperature, $T_B = 120$ K. We also recorded the μ SR spectra in presence of 45 kOe of applied longitudinal field, as depicted in fig. 2(b).

In order to elucidate the magnetic state of the sample at different T 's, we have fitted the time domain data with the double exponential function stated in eqn. 1. The

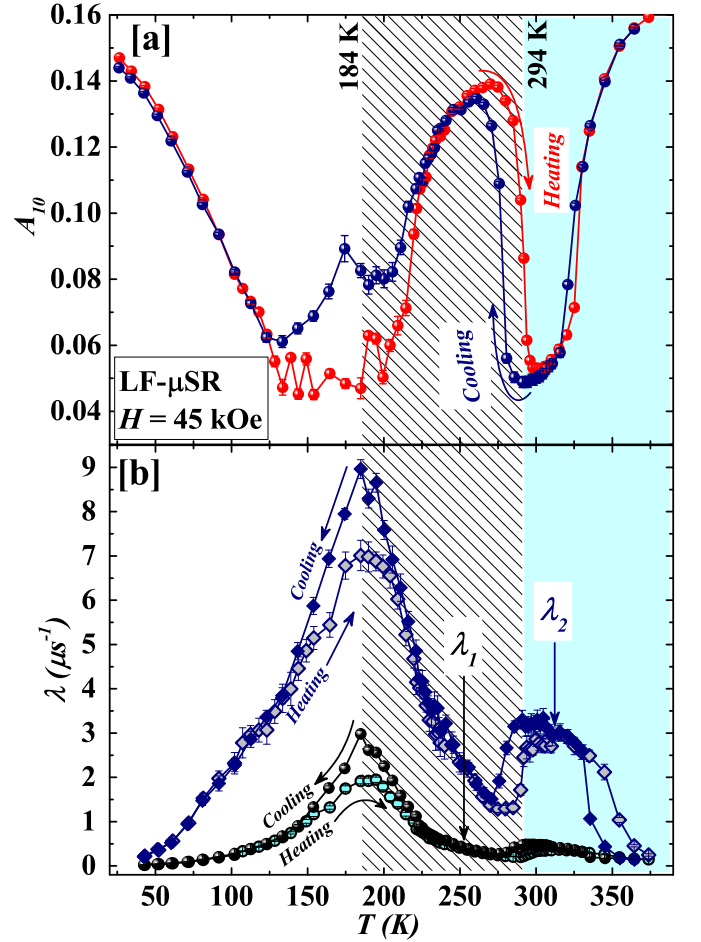


FIG. 4. (a) shows the muon asymmetry, A_1 as a function of temperature measured in 45 kOe of longitudinal magnetic field. (b) shows the thermal variation of muon depolarization rate, λ_1 and λ_2 at $H = 45$ kOe.

solid lines in figs. 2(a) and (b) represent the fit to the data. The values of A_{10} and (λ_1, λ_2) , obtained by fitting the ZF data, are plotted in figs. 3(a) and (b) respectively.

The T variation of A_{10} [see fig.3 (a)] provides noteworthy information on the magnetic state of the studied alloy. In the PM state (above 310 K), the initial asymmetry is found to be almost T independent. On cooling, A_{10} falls sharply with the onset of ferromagnetism at T_{CA} , and it attains its lowest value just below 300 K. The structural transition is beautifully echoed in that data, as A_{10} again rises sharply below T_{MS} and attains a value ($= 0.11$) slightly lower than the value in the high- T PM state ($= 0.13$). Below 260 K, A_{10} shows another sharp fall, which can easily be assigned to the second magnetic transition occurring at T_{CM} . The most remarkable observation is the sluggish rise (as opposed to the sharp change at magnetic Curie points) of A_{10} with decreasing T below T_B . This is an indication for the loss of magnetic order, and it nicely fits with the conjecture of a

glassy magnetic ground state of the system. It is evident that even at the lowest temperature, the value of A_{10} ($= 0.03$) is much smaller than the value observed in the high- T PM state. The T variation of λ_1 and λ_2 are plotted in fig. 3 (b). Both the parameters show well defined peaks at the long range magnetic ordering temperatures, which corroborates well with the nature of the $A_{10}(T)$ curve. It is worthwhile to mention that across the transition from PM to a magnetically ordered phase, one would expect the relaxing part of asymmetry to decrease by $\frac{1}{3}$ for a powder/polycrystalline sample in ZF measurement. The residual $\frac{2}{3}$ component in the time domain data will correspond to muon's damped oscillations due to the internal magnetic field.^{27,28} In the present case, the frequency of oscillation may be too high to be observed in the spectrometer at ISIS due to the large internal field from Mn.

We have fitted the LF relaxation curves recorded under 45 kOe, and the T variation of resulting parameter A_{10} is depicted in fig. 4(a). For the LF data, we recorded relaxation during both heating and cooling. The variation of LF $A_{10}(T)$ traces similar nature as that of ZF one. However, it provides few pieces of additional information, which are not obvious in the ZF data. Firstly, the sharp rise in A_{10} due to MPT gets shifted to a lower temperature under LF. It is well known that the magnetic field favors austenite and it reduces T_{MS} , which gets well reflected in our μ SR data. Secondly, clear thermal hysteresis is seen in $A_{10}(T)$ around the martensitic transition occurring at T_{MS} . The hysteresis is present in the plot of λ_1 and λ_2 as well [fig. 4 (b)], and it can be accounted by the first order nature of the structural transition. A second thermal hysteresis is present just below T_{CM} , which can be traced back to the similar thermal hysteresis observed in the bulk magnetization data (see fig. 1). Such hysteresis may be linked with the first order nature of the magnetic transition at T_{CM} .

Apart from the double exponential fitting (eqn. 1), we have used the stretched exponential function (as described by eqn. 2) to fit the time domain data. A stretched exponential form of muon depolarization is generally expected both above and below the spin freezing temperature (T_g). For a simple PM to SG transition, β attains a value close to unity at a temperature well above T_g . On cooling towards T_g , β decreases.³⁶ It has been found that for so-called concentrated canonical spin glasses (where there is a distribution of the frequency of fluctuation of the local magnetic field), β attains a value of $\frac{1}{3}$ at T_g .³⁴

We find that both the ZF and LF relaxation data can also be fitted well with a stretched exponential function as described in eqn. 2 below about 150 K. In fact the quality of the fittings in the temperature range 30-150 K is found to be better (as evident from the lower values of χ^2 of the fits) in case of stretched exponential as compared to two exponential function. However, stretched exponential fitting turns poorer above 150 K, and it fails to converge with physically meaningful values of the fitting parameters. In figs. 5 (a), (b), and (c), we have

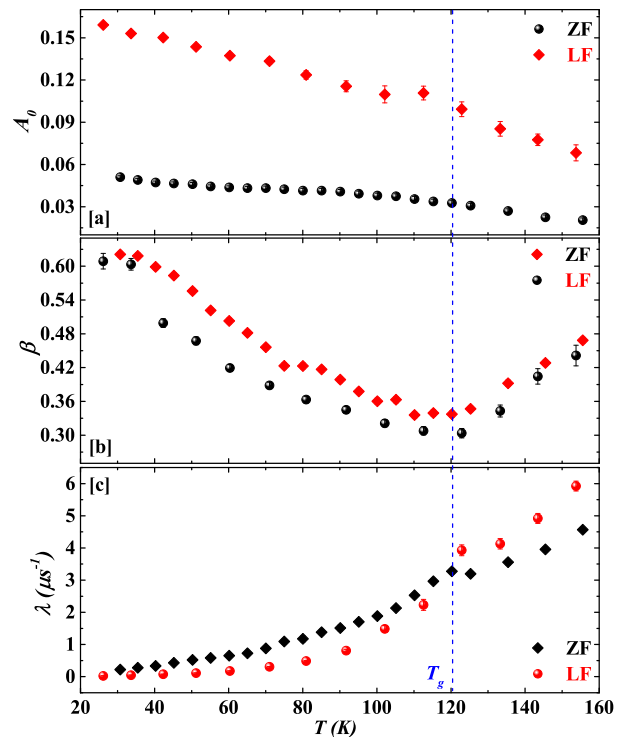


FIG. 5. (a), (b) and (c) respectively represent the temperature variation of initial asymmetry (A_0), exponent (β) and relaxation rate (λ) as obtained from fitting the time domain data using stretched exponential function as described in eqn. 2 Both ZF and LF (50 kOe) data are represented in the plots.

shown the T variations of the parameters A_0 , β and λ respectively only below 150, which were obtained by fitting the ZF and LF relaxation data recorded while the sample is being cooled. The initial asymmetry (A_0) shows a rise below 150 K, similar to the behavior of A_{10} obtained from the two exponential model. The exponent β decreases as we approach T_B from high temperature, and shows a minimum at 120 K [fig. 3 (c)]. The values β at T_B are found to be $\beta(\text{ZF})_{T_B} = 0.33(4)$ and $\beta(\text{LF})_{T_B} = 0.30(6)$. These values are fairly close to the $\beta = \frac{1}{3}$ law (particularly the ZF one) for concentrated metallic SG. Below T_B , it rises again and attains a value of 0.62 at 30 K. On the other hand, λ shows a decreasing trend on cooling along with peak like feature at T_B .

III.2. Neutron powder diffraction measurements

Figs. 6 (a), (b) and (c) show the high resolution NPD data measured at different temperatures. The sample was first heated to 363 K (which is well above T_{MS} and T_{CA}) and diffraction data were recorded while cooling from 363 to 8 K within the closed cycle refrigerator. The

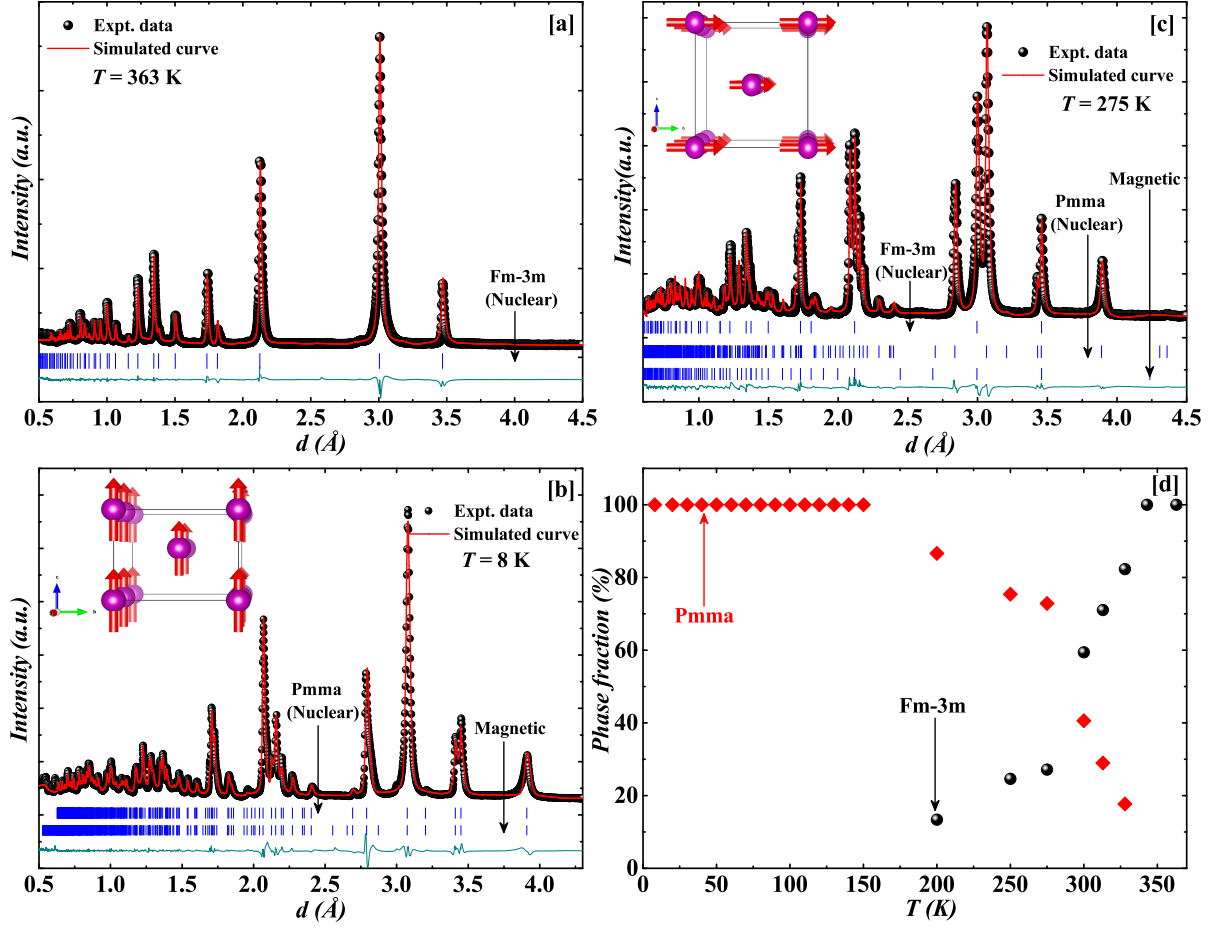


FIG. 6. (a), (b) and (c) show the powder neutron diffraction data recorded at 363 K, 8 K and 275 K respectively. The solid lines are simulated by using the FullProf suite for Rietveld refinements. (d) shows the temperature variation of martensite and austenite phase fractions as obtained from the Rietveld refinement of the neutron diffraction data.

diffraction pattern at 363 K can be well indexed by the cubic $L2_1$ structure with space group $Fm\bar{3}m$ as expected for a pure austenitic phase [see fig. 6 (a)]. At 363 K, the sample is in the PM state, and a good refinement is obtained by considering only the nuclear contribution of the cubic austenite phase with $L2_1$ geometry. The refined cubic lattice parameter is found to be $a_c = 5.991(1)$ Å. On cooling below T_{MS} , the cubic peaks start to disappear, along with the appearance of martensitic peaks [see the NPD data at 275 K in fig. 5 (c)].

At 8 K, the data can be described by a single orthorhombic phase as shown in fig. 6 (b). We do not observe any well resolved magnetic superlattice reflection, which matches well with the previous report.⁷ This rules out the possibility of an ordered AFM state below T_{MS} . In case of related Ni-Co-Mn-Ga based Heusler alloys, distinct AFM state was observed below the MPT.³⁸ A stable refinement is achieved assuming the nuclear phase coming from $Pmma$, and one magnetic phase with propagation vector $k = (0, 0, 0)$. Here we have assumed that the ordered moments arise from the Mn atoms residing at

Magnetic moment fixed along [010] direction χ^2 of fit = 6.15					
Atom	Site	X	Y	Z	moment (μ_B)
Mn	4a	0	0	0	1.780(7)
Mn	4b	0.5	0.5	0.5	1.131(5)

TABLE I. Magnetic structure data for the cubic austenite ($Fm\bar{3}m$) at 275 K as obtained from the powder neutron diffraction measurements.

$2a$ and $2f$ positions only, and neglected any contribution from Ni. We have fitted our data with several possible options of collinear magnetic structure with $k = (0, 0, 0)$, and the best fit is obtained when the moments are aligned along orthorhombic c axis. Mn atoms, situated at $2a$ and $2f$ sites, have ordered moment $2.76 \mu_B$ and $2.30 \mu_B$ respectively (see Table III).

In fig 6. (c), we have plotted NPD data for an intermediate temperature of 275 K, where both $Fm\bar{3}m$ (austenite) and $Pmma$ (martensite) phases coexist, and we have considered both the phases to refine the diffraction data. As evident from our μ SR data, the asymmetry rises below T_{MS} , indicating a PM martensitic phase. However, the residual austenite fraction may still be present in the sample having an ordered FM state. Our effort to fit 275 K data considering only the nuclear contributions coming from cubic and orthorhombic phases do not provide a good convergence. A better fit is obtained, when the FM contribution from the cubic phase is taken into consideration. Fig 6 (c) shows the experimental data as well as the refinements. The ratio of the volume fraction of the cubic and orthorhombic phases is found to be $\frac{2}{3} : \frac{1}{3}$. This indicates that below T_{MS} , the major phase fraction is martensite, although a sizable austenite phase is still present. The cubic and orthorhombic lattice parameters are found to be $a_c = 5.991(7)$ Å and $a_o = 8.613(4)$ Å, $b_o = 5.675(6)$ Å, $c_o = 4.360(5)$ Å respectively. The ordered Mn moments are found to be 1.78 and 1.13 μ_B at 4a and 4b sites respectively (see Table I). These moment values match quite well with the previous report.⁷

Interestingly, a fraction of high- T austenite continues to exist over a wide temperature range well below T_{MS} . Eventually, the reflections due to austenite disappears when the sample is cooled below 200 K. In order to determine the T variation of phase fraction, we have performed structural refinements of the NPD data at different temperatures between 8 K and 363 K. Considering the coexistence of the cubic and the orthorhombic phases, the data were refined using two phases. Fig. 6 (d) shows how the fraction of orthorhombic and cubic phases changes with T . As expected, the cubic fraction diminishes rapidly on cooling and disappears below 200 K. The orthorhombic phase fraction, on the other hand, increases monotonically and almost saturates below 150 K. It is to be noted that the thermal hysteresis in the magnetization and μ SR data disappears below 150 K. Therefore, 150 K can be assigned as the culminating point of MPT, below which the system attains a stable martensite fraction.

IV. DISCUSSIONS

The complex magnetic phases of the studied alloy get reflected in the μ SR data and in association with the NPD result, it clarifies significantly the prevailing doubts on the magnetic states of such Ni-Mn-Z based MSMA's. We observe that the values of A_{10} obtained from the μ SR data (both ZF and LF) show a sharp rise on cooling below T_{MS} , which continues till the second magnetic transition at T_{CM} is attained. The bulk magnetic measurements [as depicted in figs. 1(a) and (b)] indicate a rapid fall of M below T_{MS} , which can be due to the development of a (i) long range ordered AFM state, (ii) long range ordered FM state albeit with highly reduced Mn moment, (iii) a state with short range AFM correlations, (iv) ordered

FM clusters in the backdrop of a PM state, or (v) a pure PM state.

This sharp rise in A_{10} below T_{MS} summarily rejects cases (i) and (ii), as long range order should not be accompanied with increasing asymmetry. Therefore, we are left with options (iii), (iv) and (v). If we look at the variation of $A_{10}(T)$, the asymmetry does not fully attain its austenite PM state value just below T_{MS} . Therefore, the scenario of a pure PM state can be excluded. The magnetic state just below T_{MS} can be either due to the presence of AFM phase fraction, or associated with the residual FM austenite phase which remained untransformed even below T_{MS} . In our NPD data, we find clear signature of this cubic austenite down to 200 K. Therefore the mismatch of A_{10} at 264 K ($\approx T_{CM}$) and 350 K in the ZF μ SR data is likely to be associated with this cubic FM fraction. The variation of $A_{10}(T)$ in the LF μ SR data is somewhat similar, although the signature of T_{MS} has shifted slightly to lower temperature. This is due to the fact that an external magnetic field prefers the ferromagnetically ordered austenite.^{39,40} Logically, the most probable scenario is case (iv), where the transformed martensite is PM (the major phase), residing along with the untransformed FM austenite (the minor phase).

The thermal hysteresis around the martensitic transition is expected, and it is present in the μ SR data too. Interestingly, both $M(T)$ and $A_{10}(T)$ show another thermal hysteresis between 150 and 225 K. There are several reports on two-step martensitic transition, where a second inter-martensite transformation occurs.^{41,42} In case of one such Ni-Mn-In based alloy, the inter-martensite transition was found to occur just below T_{CM} , and it was assigned to a transformation from 10M modulated structure to 14M.⁴³ We carefully looked at the NPD data in this temperature range, however, no anomaly was detected in the form of peak splitting or appearance of additional reflections. The magnetic transition at around T_{CM} is certainly a first order one, however, it may be an iso-structural one where the lattice symmetry remains unaltered.

The most important observation in the present work is the signature of T_B in the μ SR data. As evident [see Figs. 3(a) and 4 (a)], the initial asymmetry shows a rise below T_B indicating the loss of magnetic order in the system. Notably, this rise is present irrespective of the fitting function used (two-exponential or stretched exponential). If we look at the variation of β [see fig. 5 (b)], it shows a minimum at $T_B = 120$ K with the value of β close to 0.33. In addition, λ shows a weak peak [see fig. 5 (b)] around T_B . Considering the glassy magnetic state observed in the family of Ni-Mn-Sn alloys below T_B , we can assign T_B to be the spin freezing temperature of the presently studied sample.

It is now pertinent to discuss the nature and origin of SG ground state. From our NPD data, we observe a single phase orthorhombic martensite at the base temperature. Therefore, the spin-freezing is not related to

Atom	Site	X	Y	Z	B_{iso}
Ni	4h	0.0000	0.249(6)	0.5000	1.229(7)
Ni	4k	0.2500	0.2484(4)	0.091(5)	0.544(4)
Mn	2a	0.0000	0.0000	0.0000	1.616(6)
Mn	2f	0.2500	0.5000	0.574(7)	1.500(5)
Mn	2b	0.0000	0.5000	0.0000	0.990(4)
Mn	2e	0.2500	0.0000	0.562(6)	0.990(4)
Sn	2b	0.0000	0.5000	0.0000	0.990(4)
Sn	2e	0.2500	0.0000	0.562(6)	0.990(4)

TABLE II. Crystallographic parameter of the sample at 8 K ($Pmma$) as obtained from the refinements.

Magnetic moment fixed along [001] direction χ^2 of fit = 5.45					
Atom	Site	X	Y	Z	moment (μ_B)
Mn	2a	0	0	0	2.761(6)
		0.5	0	0	
		0.25	0.5	0.574	
Mn	2f	0.75	0.5	0.574	2.302(5)
		0.75	0.5	0.574	

TABLE III. Magnetic structure of the orthorhombic martensite phase ($Pmma$) as obtained from the powder neutron diffraction measurements at 8 K.

the presence of minority cubic phase in the system. In Ni-Mn-Z based MSMAs, the sign and strength of magnetic interaction depend strongly on the Mn-Mn bond distance. Below T_{MS} , the intersite Mn-Mn' distance decreases paving the path for enhanced AFM correlation.^{8,11,14,44} In addition, chemical and lattice disorders play an important role in determining the magnetic ground state of these materials.¹¹ The AFM correlations between Mn-Mn' (particularly below T_{MS}), the Mn-Mn FM correlations and the presence of disorder eventually lead to spin freezing below T_B . The Mn' atoms are substituted randomly in the Sn site, which can give rise to random occurrence of FM and AFM bonds. From our analysis of the NPD data it is evident that the AFM correlations is short range in nature, *i.e.*, it does not give rise to a long range ordered AFM state. Nevertheless, the ground state does show long range FM order.

In general for a PM to SG transition, the value of β in the stretched exponential fitting assumes a constant value below the spin freezing temperature due to the residual fluctuation of the frozen state.³⁵ In contrary to the usual observation, the value of β increases below T_B and attains a value of 0.62 at 30 K. The main reason for such anomalous behavior of β lies with the reentrant character of the SG state, where spin freezing takes place on top of a long range FM state. Interestingly, very similar T dependence of β was reported in case of $Pb(Fe_{1/2}Nb_{1/2})O_3$, where β shows a minimum at $T_g = 20$ K and approaches

to unity on further cooling.³⁷ The SG state in this compound is reentrant type which develops in the backdrop of an AFM state. It has been argued that with the critical slowing down of the SG fluctuations at T_g , muons starts to sense the non-critical fluctuations of the long range ordered state below T_g leading to the increase in β . By analogy, the rise in β below T_B in the studied Ni-Mn-Sn alloy can be accounted by the presence of long range ordered FM phase with the SG state side by side. This is corroborated by the NPD data, where FM order is indeed present at 8 K. The weak nature of the peak in $\lambda(T)$ data (ideal spin glass should show a sharp peak at spin freezing temperature) may be due to the presence of this FM ordered state alongside the SG phase.

In conclusion, the present work successfully discerns few ambiguities related to the magnetic phase diagram of Ni-Mn-Sn alloy system. Based on our study on a particular Ni-Mn-Sn alloy, it is evident that the alloy assumes a PM state just below the martensitic transition. The μ SR result identifies two long range magnetic ordering temperatures T_{CA} , and T_{CM} and they are found to be ferromagnetic in nature. The work categorically justifies the view that the magnetic anomaly at T_{CM} in the martensitic state indeed corresponds to the onset of a long range ordered state. Most importantly, the work identifies that the system transform into a partially disordered magnetic phase below the exchange bias blocking temperature, which can be characterized by the coexistence of ordered FM and frozen spin glass state. The remarkable phenomena of exchange bias observed in Ni-Mn-Z alloys is due to the coupling between the interfacial spins of SG and FM phases.

V. ACKNOWLEDGMENT

The work is supported by the India-RAL collaborative project (SR/NM/Z-07/2015). J. Sannigrahi wishes to acknowledge EUs Horizon 2020 research and innovation programme under the Marie Skłodowska-Curie Grant Agreement (No. 665593) awarded to the STFC, UK.

-
- * sspsm2@iacs.res.in
- ¹ R. Kainuma, Y. Imano, W. Ito, Y. Sutou, H. Morito, S. Okaoto, O. Kitakami, K. Oikawa, A. Fujita, T. Kanomata, and K. Ishida, *Nature* **439**, 957 (2006).
 - ² T. Krenke, E. Duman, M. Acet, E. F. Wassermann, X. Moya, L. Mañosa, and A. Planes, *Nat. Mater.* **4**, 450 (2005).
 - ³ R. Kainuma, K. Oikawa, W. Ito, Y. Sutou, T. Kanomata, K. Ishida, *J. Mater. Chem.* **18**, 1837 (2008).
 - ⁴ L. Mañosa, X. Moya, A. Planes, T. Krenke, M. Acet, E. F. Wassermann, *Materials Science and Engineering A* **481-482**, 49 (2008).
 - ⁵ S. Chatterjee, S. Giri, and S. Majumdar, and S. K. De, *Phys. Rev. B* **77**, 012404 (2008).
 - ⁶ L. Mañosa, D. González-Alonso, A. Planes, E. Bonnot, M. Barrio, J.-L. Tamarit, S. Aksoy and M. Acet, *Nat. Mater.* **9**, 478 (2010).
 - ⁷ P. J. Brown, A. P. Gandy, K. Ishida, R. Kainuma, T. Kanomata, K. U. Neumann, K. Oikawa, B. Ouladdiaf and K. R. A. Ziebeck, *J. Phys.: Condens. Matter* **18**, 2249 (2006)
 - ⁸ V. D. Buchelnikov, P. Entel, S. V. Taskaev, V. V. Sokolovskiy, A. Hucht, M. Ogura, H. Akai, M.E. Gruner, S. K. Nayak, *Phys. Rev. B* **78** (2008) 184427
 - ⁹ M. Ye, A. Kimura, Y. Miura, M. Shirai, Y. T. Cui, K. Shimada, H. Namatame, M. Taniguchi, S. Ueda, K. Kobayashi, R. Kainuma, T. Shishido, K. Fukushima, and T. Kanomata, *Phys. Rev. Lett.* **104**, 176401 (2010)
 - ¹⁰ C.L. Tan, Y.W. Huang, X.H. Tian, J.X. Jiang, W. Cai, *J. Appl. Phys.* **100** (2012) 132402.
 - ¹¹ V. V. Sokolovskiy, V. D. Buchelnikov, M. A. Zagrebin, P. Entel, S. Sahoo, and M. Ogura, *Phys. Rev. B* **86**, 134418 (2012)
 - ¹² H. B. Xiao, C. P. Yang, R. L. Wang, V. V. Marchenkov, and X. Luo, *J. Appl. Phys.* **115**, 203703 (2014)
 - ¹³ C.-M. Li, Q.-M. Hu, R. Yang, B. Johansson, and L. Vitos, *Phys. Rev. B* **92**, 024105 (2015).
 - ¹⁴ K. R. Priolkar, P. A. Bhobe, D. N. Lobo, S. W. DSouza, S. R. Barman, Aparna Chakrabarti, and S. Emura, *Phys. Rev. B* **87**, 144412 (2013)
 - ¹⁵ R. Y. Umetsu, R. Kainuma, Y. Amako, Y. Taniguchi, T. Kanomata, K. Fukushima, A. Fujita, K. Oikawa, and K. Ishida, *Appl. Phys. Lett.* **93**, 042509 (2008)
 - ¹⁶ P. J. Brown, A. P. Gandy, R. Kainuma, T. Kanomata, K. U. Neumann, K. Oikawa, B. Ouladdiaf, A. Sheikh and K. R. A. Ziebeck, *J. Phys.: Condens. Matter* **23**, 456004 (2011)
 - ¹⁷ S. Aksoy, M. Acet, P. P. Deen, L. Mañosa and A. Planes, *Phys. Rev. B* **212401** (2009).
 - ¹⁸ S Chatterjee, S Giri, SK De, and S Majumdar, *Phys. Rev. B* **79**, 092410 (2009).
 - ¹⁹ D. Y. Cong, S. Roth, J. Liu, Q. Luo, M. Pötschke, C. Hürlich, and L. Schultz, *Appl. Phys. Lett.* **96**, 112504 (2010)
 - ²⁰ B. M.Wang, Y. Liu, P. Ren, B. Xia, K. B. Ruan, J. B. Yi, J. Ding, X. G. Li, and L.Wang, *Phys. Rev. Lett.* **106**, 077203 (2011)
 - ²¹ R Y Umetsu, A Fujita, W Ito, T Kanomata, and R Kainuma, *J. Phys.: Condens. Matter* **23**, 326001(2011)
 - ²² M. K. Ray, K. Bagani, P. K. Mukhopadhyay, and S. Banerjee, *EPL* **109**, 47006(2015).
 - ²³ S. Pramanick, S. Chatterjee, S. Giri, and S. Majumdar, *Appl. Phys. Lett.* **105**, 112407 (2014).
 - ²⁴ S. Pramanick, S. Chattopadhyay, S. Giri, and S. Majumdar, S. Chatterjee, *J. Appl. Phys.* **116**, 083910 (2014)
 - ²⁵ <https://www.ill.eu/sites/fullprof/>
 - ²⁶ S. J. Blundell, *Cont. Phys.* **40**, 175 (1999).
 - ²⁷ D. H. Ryan, J. van Lierop and J. M. Cadogan, *J. Phys.: Condens. Matter* **16**, S4619 (2004)
 - ²⁸ P. Dalmas de Réotier and A. Yaouanc, *J. Phys.: Condens. Matter* **9**, 9113 (1997).
 - ²⁹ R. H. Heffner, J. E. Sonier, D. E. MacLaughlin, G. J. Nieuwenhuys, G. Ehlers, F. Mezei, S.-W. Cheong, J. S. Gardner, and H. Röder, *Phys. Rev. Lett.* **85**, 3285 (2000).
 - ³⁰ Y. Kawasaki, T. Minami, M. Izumi, Y. Kishimoto, T. Ohno, K. H. Satoh, A. Koda, R. Kadono, J. L. Gavilano, H. Luetkens, T. Nakajima, and Y. Ueda, *Phys. Rev. B* **86**, 125141 (2012).
 - ³¹ R. H. Heffner, J. E. Sonier, D. E. MacLaughlin, G. J. Nieuwenhuys, G. M. Luke, Y. J. Uemura, William Ratcliff, II, S-W. Cheong, and G. Balakrishnan. *Phys. Rev. B* **63**, 094408 (2001).
 - ³² H. Guo, K. Manna, H. Luetkens, M. Hoelzel, and A. C. Komarek, *Phys. Rev. B* **94**, 205128 (2016).
 - ³³ M. Hiroi, T. Hisamatsu, T. Suzuki, K. Ohishi, Y. Ishii, and I. Watanabe, *Phys. Rev. B* **88**, 024409 (2013)
 - ³⁴ I. A. Campbell, A. Amato, F. N. Gyax, D. Herlach, A. Schenck, R. Cywinski and S. H. Kilcoyne, *Phys. Rev. Lett.* **72**, 1291 (1994)
 - ³⁵ Y. Fudamoto, K. M. Kojima, M. I. Larkin, G. M. Luke, J. Merrin, B. Nachumi, Y. J. Uemura, M. Isobe, and Y. Ueda, *Phys. Rev. Lett.* **83**, 3301 (1999).
 - ³⁶ J. Teyssier, E. Giannini, V. Guritanu, R. Viennois, and D. van der Marel, A. Amato, and S. N. Gvasaliya, *Phys. Rev. B* **82**, 064417 (2010).
 - ³⁷ G. M. Rotaru, B. Roessli, A. Amato, S. N. Gvasaliya, C. Mudry, S. G. Lushnikov, and T. A. Shaplygina, *Phys. Rev. B* **79**, 184430 (2009)
 - ³⁸ F. Orlandi, S. Fabbri, F. Albertini, P. Manuel, D. D. Khalyavin, and L. Righi. *Phys. Rev. B* **94**, 140409(R) (2016)
 - ³⁹ K. Koyama, and Kazuo Watanabe, *Appl. Phys. Lett.* **88**, 132505 (2006).
 - ⁴⁰ A. Planes, L. Mañosa, and M. Acet, *J. Phys.: Condens. Matter* **21**, 233201 (2009).
 - ⁴¹ G. Fan, W. Chen, S. Yang, J. Zhu, X. Ren and K. Otsuka, *Acta Mater.* **52**, 4351 (2004).
 - ⁴² M.C. Carroll, Ch. Somsen, G. Eggeler, *Scr. Mater.* **50**, 187 (2004).
 - ⁴³ Y.J. Huang , Q.D. Hu, J. Liu, L. Zeng, D.F. Zhang, J.G. Li, *Acta Mater.* **61**, 5702 (2013)
 - ⁴⁴ P. Borgohain, and M. B Sahariah, *J. Phys.: Condens. Matter* **27**, 175502 (2015)